Soils and Rocks
An International Journal of Geotechnical and Geoenvironmental Engineering
www.soilsandrocks.com
ISSN 1980-9743
ISSN-e 2675-5475

Effect of anisotropic hydraulic conductivity on groundwater seepage into a rectangular tunnel in submerged sand

Deki Yangzom Ghaley[1#], Sanjay Kumar Shukla[1,2,3]

Article

Keywords
Groundwater
Tunnel seepage
Rectangular tunnel
Cohesionless soil
Flow patterns
Anisotropic hydraulic conductivity

Abstract

Managing groundwater seepage around tunnels is critical to tunnel design, particularly when the tunnel is constructed below the water table. Accurate seepage flow patterns and water inflow prediction under ordinary and critical conditions are imperative to mitigate potential tunnel construction and service disasters. In the past, an in-depth study on the anisotropic hydraulic conductivity of the soil mass that may affect the seepage condition has not been carried out. In this work, this aspect has been investigated numerically for a rectangular tunnel submerged within a homogeneous sand mass, considering the anisotropic hydraulic conductivity ratio (k_z / k_x, k_z = vertical hydraulic conductivity and k_x = horizontal hydraulic conductivity) varying from 0.25 to 1. This study has presented the changes in the flow patterns of groundwater around a rectangular tunnel for different values of k_z / k_x, and the variation of water inflow rates along the crown, invert and walls of the tunnel. The results indicate that as k_z / k_x decreases from 1 to 0.25, the water inflow rate into the tunnel reduces linearly and the invert of the tunnel experiences the highest inflow rate. The total water inflow into the tunnel when k_z / k_x = 1 is three times the inflow rate for k_z / k_x = 0.25. An illustrative example has been included to help tunnel designers and construction engineers utilize the findings of this study for practical lining and permanent tunnel drainage systems.

1. Introduction

The primary geotechnical problem encountered during the construction and service of tunnels is groundwater inflow from water-saturated earth mass, leading to disastrous experiences (Freeze & Cherry, 1979). Estimating seepage flow into tunnels is of great significance for the design of stable liners and the drainage system, especially when the water table remains above or moves up the invert of the tunnel. When a tunnel is excavated below the groundwater level, the groundwater flows into the excavated surface of the tunnel, and a difference in hydraulic head exists around the tunnel. The force that acts on the soil particle due to the differential head is known as the seepage force, and it is exerted in the direction of groundwater flow (Shukla, 2014; Lee et al., 2003), especially in homogeneous and isotropic soil masses. The entry of water into tunnels gives rise to several notable challenges, such as compromising the stability of the surrounding rock mass, exerting additional pressure on temporary and permanent support structures, diminishing operational speed, causing adverse environmental impacts, and causing financial implications (Farhadian et al., 2012; El Tani, 2003). Engineers need estimates of tunnel groundwater inflow to design the tunnel drainage systems (Butscher, 2012).

To cope safely with large groundwater inflows into tunnels, it is essential to develop reliable methods to predict its quantities in advance (Freeze & Cherry, 1979). A diverse approximation of water inflow has been conducted by Muskat (1937), Goodman et al. (1965), Rat (1973), Schleiss (1988), Lei (1999) and Karlsrud (2001), considering a circular tunnel in a homogeneous and isotropic aquifer. El Tani (2003) solved the steady-state gravity flow generated by a circular tunnel in a semi-infinite, homogeneous, and isotropic aquifer using Mobius transformation and Fourier series. Kolymbas & Wagner (2007) derived an analytical expression for estimating steady-state groundwater inflow into drained circular tunnels based on conformal mapping and allocating variable total head along the tunnel circumference, which is valid for deep and shallow tunnels. Park et al. (2008) presented a comparison of the existing analytical solutions by Muskat (1937), Goodman et al. (1965), Rat (1973), Schleiss (1988) and Lei (1999) with their exact analytical solution of steady-state groundwater inflow into a drained circular tunnel located in a semi-infinite aquifer for two different boundary conditions by using conformal mapping technique.

[#]Corresponding author. E-mail address: dghaley@our.ecu.edu.au
[1]Edith Cowan University, School of Engineering, Geotechnical and Geoenvironmental Engineering Research Group, Perth, WA, Australia.
[2]Delhi Technological University, Department of Civil Engineering, Delhi, India.
[3]VR Siddhartha Engineering College, Department of Civil Engineering, Vijayawada, India.

Submitted on August 1, 2025; Final Acceptance on December 3, 2025; Discussion open until November 30, 2026.
Editor: Renato P. Cunha
https://doi.org/10.28927/SR.2026.012525

Yang et al. (2015) proposed an analytical solution for water inflow into a subsea tunnel, considering the surrounding rock parameters, lining, and grouting. Furthermore, Liu & Li (2021) derived an analytical solution for groundwater inflow into lined circular tunnels considering waterproofing and drainage systems. Lee & Nam (2001) investigated the impact of seepage forces on tunnel linings for circular drainage-type and waterproof tunnels situated in alluvial soil. Their numerical analysis highlighted the importance of accounting for groundwater conditions in the safe and reliable design of tunnels. The linings must be designed for waterproof tunnels to withstand the hydrostatic load. Even for drainage-type tunnels, the linings should be designed to support hydrostatic loads under steady-state flow conditions, a factor that is often overlooked in current design practices. The studies conducted by these researchers were only for circular tunnels in a homogeneous, isotropic aquifer with a horizontal water table. In 2021, Li et al. (2021) developed a semi-analytical solution for steady-state groundwater inflow into a circular tunnel considering the anisotropic permeability of the surrounding soil mass based on coordinate transformation and conformal mapping for two different boundary conditions. Dong et al. (2020) provided an analytical solution for groundwater inflow in an unlined non-circular tunnel in an infinite plane using a conformal mapping technique.

While numerous studies have investigated groundwater inflow in circular and non-circular tunnels, to the authors' best knowledge, there appears to be limited research specifically addressing groundwater flow in rectangular tunnels under anisotropic hydraulic conductivity. Rectangular tunnels are now considered for urban road and railway underpasses as it provides higher space utilization than the circular cross-section of the same excavation width leading tunnel designers to favor these geometries in constrained city environments. (Ma et al., 2024). Published case histories include super-large rectangular tunnels constructed beneath existing urban infrastructure in China, where the rectangular cross-section is opted to maximize the usable roadway width (Ma et al., 2023). In many of these urban settings, anisotropic hydraulic conductivity of the ground naturally arises due to layered soil deposits, which can significantly impact the seepage patterns around tunnels. Anisotropic hydraulic conductivity arises when the conductivity in the horizontal and vertical directions is different. The soil, in its natural condition, is often observed to be rarely homogeneous (Smith, 1981). The variation in conductivity based on direction arises from the soil's structure and how it was deposited. Under the influence of gravity, soil particles settle with their major axis aligned horizontally. Generally, in homogeneous natural deposits and in soil layers that have not been disturbed or rotated by tectonic forces over time, the conductivity in the horizontal direction is always greater than in the vertical direction (Harr, 1962; Smith, 1981; Nova, 2010), which is a critical factor in conventional groundwater seepage analysis. Wei et al. (2022) explored seepage fields around twin non-circular tunnels in permeable, anisotropic ground, considering the effect of varying the anisotropic permeability ratio. However, their study did not address the influence of anisotropic permeability on single rectangular tunnels, which leaves a gap for exploration. Hence, in this study, an attempt has been made to study the effects of anisotropic hydraulic conductivity of soil on the behavior of groundwater flow into a single rectangular unlined tunnel through numerical modeling using the SEEP/W module of GeoStudio 2023.1.0. Understanding the water flow characteristics (Ishibashi & Hazarika, 2010), like flow patterns, hydraulic head distribution, and porewater pressure distribution around tunnels, is essential for designing and constructing tunnel linings and drainage systems effectively and assessing environmental impacts. The findings of this research will provide valuable insights for practicing tunnel engineers, enhancing their approach to lining and permanent drainage design and environmental impact assessment.

2. Numerical model

2.1 Model geometry and assumptions

Unlike analytical solutions, a numerical model helps flexibly represent complex geological conditions of an actual site by incorporating varying hydraulic properties and boundary conditions (Butscher, 2012) and transient conditions (Font-Capo et al., 2011). This capability is valuable for applications requiring the differentiation between the water inflow at the invert and crown of the tunnel (Butscher et al., 2011a). In tunnel engineering, the advancement of computational performance of computers boosted the use of finite element modeling for groundwater models (Bear, 1972).

In this study, an arbitrary rectangular unlined tunnel within a submerged, homogeneous, anisotropic, saturated sand mass was considered to analyze groundwater flow patterns around it using the SEEP/W module of GeoStudio 2023.1.0. SEEP/W is designed based on the principle that the movement of water in both saturated and unsaturated soil adheres to Darcy's Law (GEO-SLOPE, 2015). This law states that the rate of flow through soil is proportional to the hydraulic gradient and the hydraulic conductivity of soil, as given below:

$$q = ki \tag{1}$$

The governing equation for the steady-state seepage in anisotropic soil mass is given by the Laplace's equation as given below (Terzaghi et al., 1996; Shukla, 2025):

$$k_x \frac{\partial^2 h}{\partial x^2} + k_z \frac{\partial^2 h}{\partial z^2} = 0 \tag{2}$$

The following assumptions have been considered for the analysis:

1) The groundwater flow is steady.
2) The water table does not fluctuate and is horizontal, assuming a constant recharge of the groundwater into the soil mass.
3) The soil mass may exhibit anisotropic hydraulic conductivity, which means that the hydraulic conductivity in the horizontal direction may differ from that in the vertical direction.

Figure 1 represents the two-dimensional model geometry of dimensions 50 m × 50 m, with the tunnel located below the water table in a semi-infinite soil mass. For simplicity, the soil mass above the water table was also assumed to be fully saturated. The value of the saturated hydraulic conductivity of the soil mass has been taken as 1×10^{-3} m/s, corresponding to the value of coarse sand mass. Multiple analyses have been carried out to study the effects of varying k_z / k_x.

2.2 Boundary conditions, meshing patterns, and validation

In the model shown in Figure 1, the top and sides were considered permeable boundaries, allowing water to pass through. A constant total head boundary condition was applied to these surfaces to simulate water flow under steady-state conditions. Meanwhile, the bottom of the model was considered impermeable, assuming no water could flow through it, and a no-flow boundary condition was applied. This application of the boundary conditions simulates a scenario where water can infiltrate through the top and sides but is blocked from escaping through the bottom.

Regarding the tunnel, zero water pressure was assumed along its surface, representing a condition where the tunnel lacks any lining. Without lining, the tunnel is exposed directly to the surrounding environment. Inside the tunnel, the internal pressure was assumed to be atmospheric, as no protective barrier alters the pressure conditions. This assumption allows for evaluating seepage behavior under the specific condition of an unlined tunnel in contact with groundwater.

The meshing pattern adopted in the numerical model is a mixture of quads and triangles consisting of 534 nodes and 497 elements with a global element size of 2.9 m, as shown in Figure 2. This pattern generates mostly quadrilateral elements with fewer triangular elements wherever necessary, to provide a smooth transition and proper element shape quality (GEO-SLOPE, 2015). This meshing pattern was chosen given its ability to be used with any region shape. A sensitivity analysis was carried out to validate the selection of the mesh size, and the results obtained do not make any remarkable difference in the inflow rate into the tunnel.

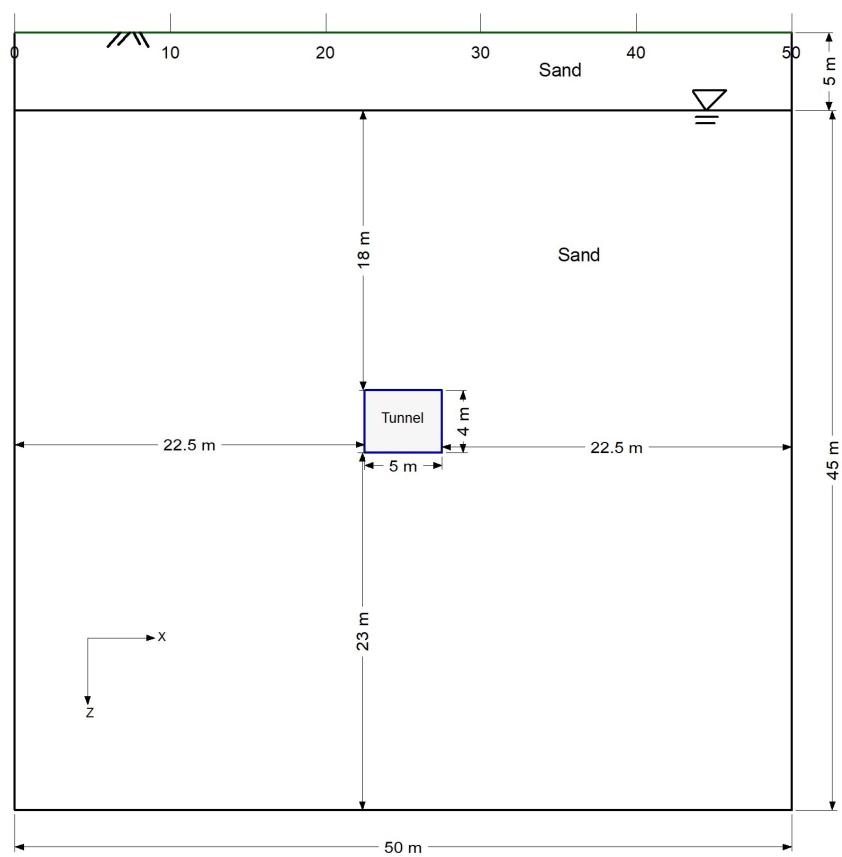

Figure 1. Rectangular unlined tunnel below the water table.

It is pertinent to check the accuracy of the numerical model to ensure its credibility. In general, a numerical model is validated using the experimental and/or field results, but data are hardly available for seepage problems in rectangular tunnels. Moreover, to the best of the authors' knowledge, the analytical expression for seepage into a rectangular tunnel is missing in the literature. Therefore, in this case, the result from the numerical analysis was validated using some of the well known analytical solutions as presented in Table 1. The solution provided by Goodman et al. (1965) and Su et al. (2017) are for circular tunnels and by El Tani (1999) is for a square tunnel. Therefore, in this study, the area and perimeter of the rectangular tunnel is equated to the area and circumference/perimeter of circular/square tunnel and the results are shown in Table 1.

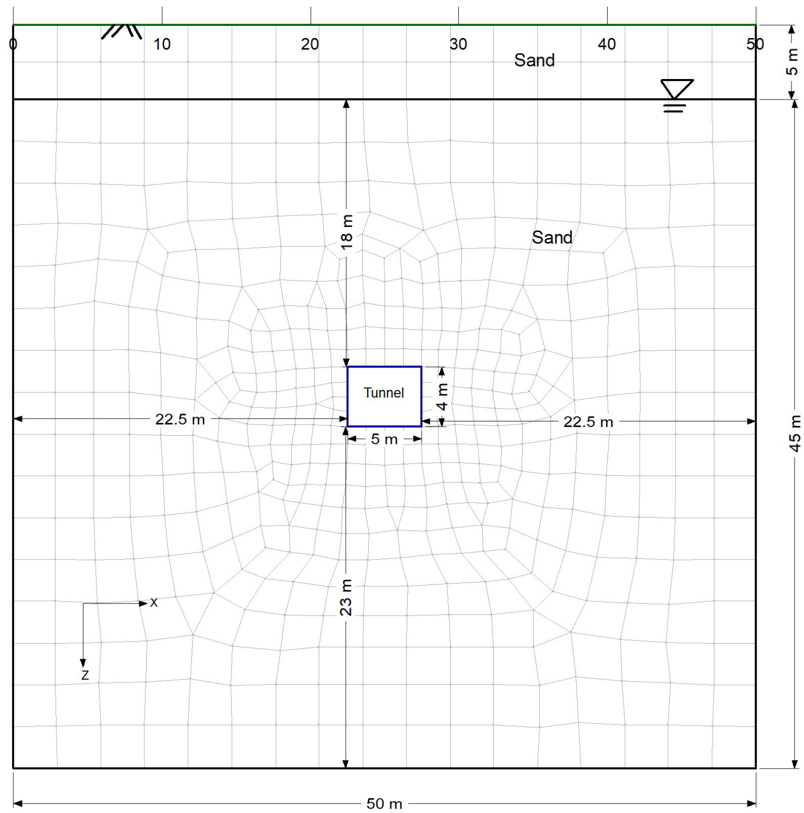

Figure 2. Finite element mesh (FEM) around the tunnel.

Table 1. Comparison of the water inflow rates.

Analytical method	Water inflow rate per m length of tunnel, q ($\times 10^{-2}$)			Reference
	Equivalent cross-sectional area method (m^3/s)	Equivalent perimeter method (m^3/s)	Numerical method (m^3/s)	
$q = \dfrac{2\pi k h_0}{2.3\log\left(\dfrac{2h_0}{r}\right)}$	4.6	4.7		Goodman et al. (1965)
$q = \dfrac{2\pi k h_0}{\dfrac{6-\pi}{4} + ln\left(\dfrac{2^{0.75} h_0}{a}\right)}$	3.4	4.6	3.2	El Tani (1999)
$q = 2\pi k \dfrac{0.3\left(\dfrac{r}{h_0}\right)^{-0.014r-0.22} h_0}{ln\dfrac{2h_0}{r}}$	2.3	2.4		Su et al. (2017)

Legend: see List of symbols and abbreviations.

The numerical result exhibits close agreement with the analytical solution of El Tani when the equivalent cross-sectional method is employed, with a relative difference of approximately 5% as given in Figure 3. Among the three analytical solutions considered, El Tani's approach is formulated specifically for square cross-sections. The strong correspondence between the numerical and El Tani's analytical results in this study is attributed to the use of a rectangular cross-section, which closely resembles square geometry. This agreement suggests that the model setup, boundary conditions, and meshing strategy effectively replicate the hydraulic conditions described by El Tani (1999).

3. Results and discussion

3.1 Flow nets and flux vectors

A flow net is a graphical representation of a flow field that satisfies Laplace's equation of continuity as given in Equation 2 (Budhu, 2007; Das & Sobhan, 2012) and is a map of contours having flow lines and equipotential lines (GEO-SLOPE, 2015; Aysen, 2006). It is an effective tool for analyzing groundwater movement through the soil, as it helps visualize the seepage patterns and contributes to the design process and stability assessment (Rocscience Inc., 2023).

Flow lines are paths followed by groundwater through the soil, which never cross each other, and equipotential lines are the lines joining points of equal pressure head (Smith, 2013; Shukla, 2014; Powrie, 2017). Depending on the convenience, infinite flow paths and equipotential lines can be drawn. Flow nets provide a visualization of how groundwater moves around the tunnel and through the surrounding soil mass. This is important for estimating the flow rate of water seeping into the tunnel to design an effective drainage system. Furthermore, it helps optimize the design of tunnel linings, ensuring that the lining is sufficiently designed to withstand groundwater pressure. A flow net generated by the software after analysis is shown in Figure 4.

The direction and magnitude of groundwater flow through the soil mass and around the tunnel are represented visually using flux vectors, as shown in Figure 5. These vectors provide a clear understanding of how water moves through the surrounding soil, helping to analyze seepage behavior and design appropriate control measures. The arrows of the flux vectors point in the direction of groundwater flow. This means that at each location in the model, the arrow's direction corresponds to the path water takes through the porous media. Depending on the flow conditions, these vectors illustrate how water is drawn toward or away from the tunnel. The length of the flux vectors is directly proportional to the magnitude of groundwater flow at a given location. Longer arrows indicate areas with higher water inflow through that region over a specific amount of time. However, shorter arrows represent areas of lower water inflow. This graphical representation provides a clear understanding of how water behaves across different parts of the model. The flux vectors typically show higher flow rates in the area close to the tunnel surface. This is because water tends to concentrate near the tunnel, especially if it is unlined and is subjected to direct contact with groundwater. Hence, understanding the behavior of these flux vectors is essential for assessing the tunnel's structural stability and seepage management strategies, as areas having high flow rates may require rigorous drainage solutions to mitigate water intrusion.

3.2 Distribution of hydraulic head

The contours of the hydraulic head around the tunnel are shown in Figure 6. Each line represents points having a constant hydraulic head value. The contour lines are closer together around the vicinity of the tunnel and are farther apart as we move away from the tunnel.

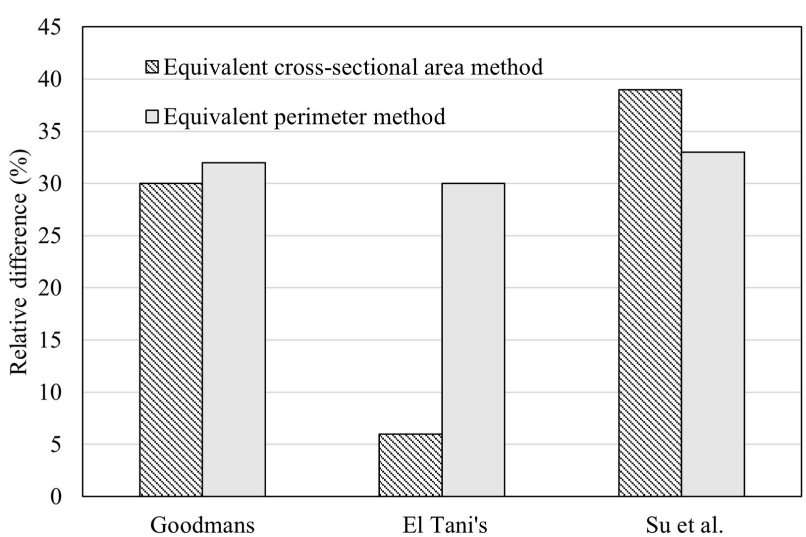

Figure 3. Comparison of results.

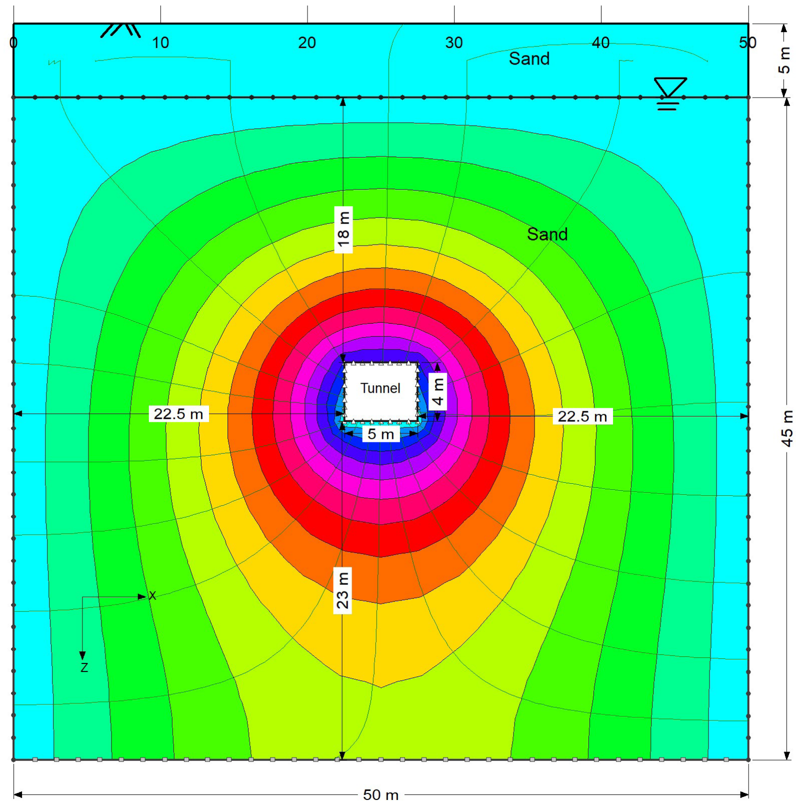

Figure 4. Flow net for $k_z / k_x = 1$.

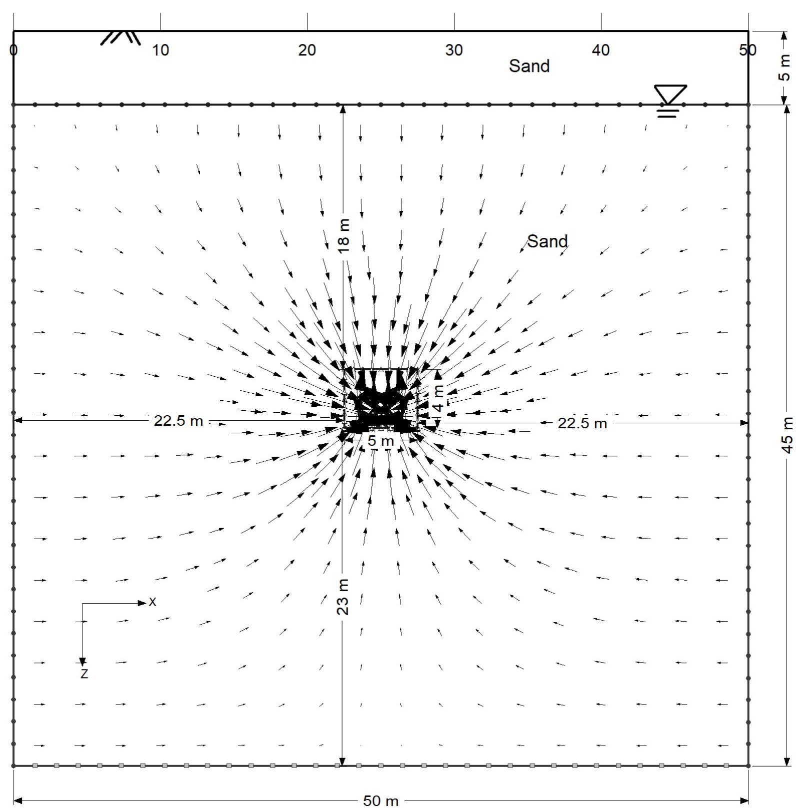

Figure 5. Flux vector for $k_z / k_x = 1$.

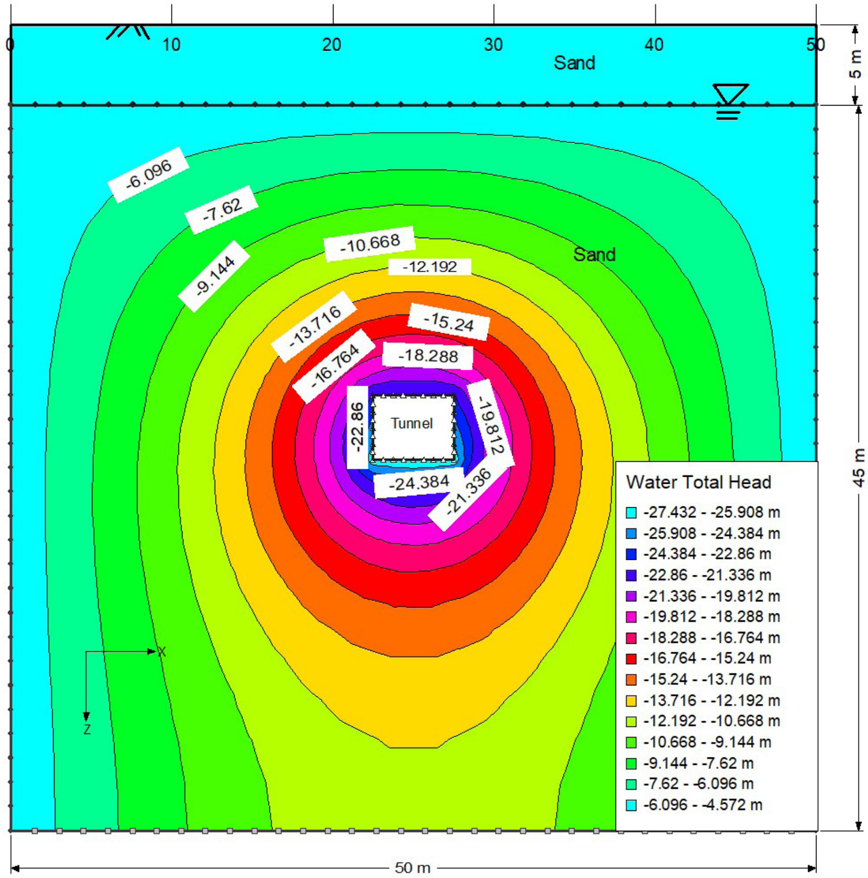

Figure 6. Hydraulic head distribution for $k_z / k_x = 1$.

This signifies that the hydraulic gradient is steeper near the tunnel, which relates to rapid change in the water pressure. The seepage rate is expected to be higher in areas where the contour lines are close together. The spreading out of the contour lines indicates a gentler hydraulic gradient, which indicates that the effect of the tunnel on the groundwater flow is minimal. In these areas, the groundwater movement is slower, resulting in a slower rate of change in the hydraulic head. However, in the case of two parallel non-circular tunnels, the contour lines are denser at the region between the tunnel crown and ground surface, indicating that the water pressure and inflow rate are higher in this region (Wei et al., 2022). This highlights the difference in the hydraulic head distribution for single and twin tunnels.

3.3 Pore-water pressure distribution around the tunnel

The contours in Figure 7 represent lines of constant pore water pressure, revealing the hydraulic gradient determining the groundwater flow direction. Steeper gradients are observed near the tunnel, which indicates that the groundwater will flow quickly towards the tunnel. Shallower gradients are observed further away from the tunnel, indicating slower groundwater movement as there is a gradual change in pressure. The pore water pressure increases with depth due to the weight of the overlying water column and soil. The rapid drop in the pressure around the tunnel boundary implies that water flow is converging toward the tunnel.

3.4 Effect of anisotropic hydraulic conductivity ratio

In most of the seepage analysis of the tunnel, isotropic conductivity is assumed, which means the conductivity in the horizontal and vertical directions is considered the same. However, in real-life scenarios, conductivity is not always the same in all directions. Therefore, to study the effects of k_z / k_x on the water inflow rate into the tunnel, a comparison of the hydraulic head and pore water pressure distribution around the tunnel is made, as shown in Figures 8 and 9 by decreasing the ratio from 1 to 0.75, 0.50 and 0.25. As the ratio decreases, the contour spacing gets closely packed in the horizontal direction, indicating a steeper hydraulic gradient. This indicates the effect of high horizontal hydraulic conductivity. Figure 10 illustrates the variation in the water inflow rates through the crown, invert, and the walls of the tunnel, highlighting how the inflow rates

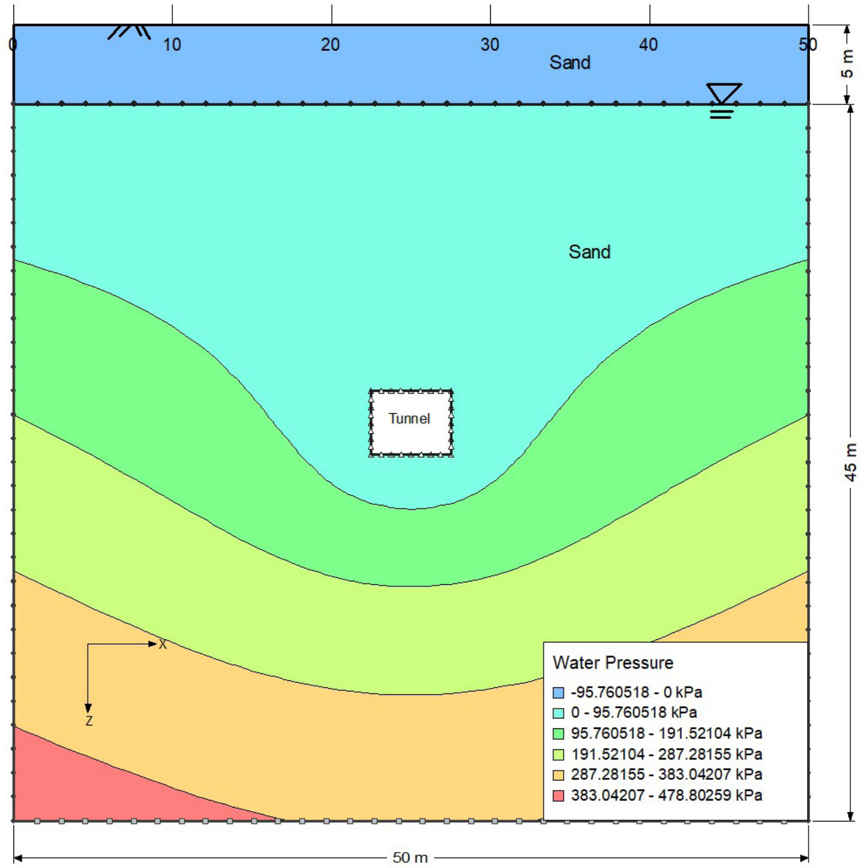

Figure 7. Pore water pressure distribution for $k_z / k_x = 1$.

change with distance for varying k_z / k_x. It can be observed that the overall trend is consistent with water inflow at the crown, invert, and walls. The water inflow rate reaches its maximum near the tunnel edges at the crown and invert, while the minimum occurs at the center. Along the tunnel walls, the maximum inflow occurs at a depth of 27 m below ground level, with the minimum at 24 m. The water inflow rate is highest when k_z / k_x is 1, corresponding to isotropic conditions, and decreases gradually as the ratio reduces. Specifically, at the crown and invert, the inflow decreases by approximately 1.2 to 2 times the isotropic case as k_z / k_x decreases. However, at the tunnel walls, the inflow rate decrease varies between 1.1 to 1.5.

Figure 11 compares how the inflow rate is affected by the decrease in the k_z / k_x values at the crown, invert, and walls of the tunnel. The reduction in the water inflow values at the crown, invert, and walls is approximately linear with the decrease in k_z / k_x values. The invert exhibits the highest water inflow rate across all values of k_z / k_x, which indicates that the bottom of the tunnel receives more water inflow than the other sections, probably due to the pressure exerted by groundwater beneath the tunnel. This is like the case of a circular tunnel located in a soil mass exhibiting anisotropic hydraulic conductivity when zero water pressure is considered along the tunnel surface (Li et al., 2021). The tunnel walls exhibit a moderate water inflow rate, lower than the invert but higher than the crown. The crown experiences the least water inflow rate compared to the invert and the walls. Figure 12 presents the variation of the overall water inflow rate per meter length of tunnel with the decrease in the hydraulic conductivity ratio. When k_z / k_x is 0.75, the total inflow rate is 1.2 times lower than the isotropic case. Similarly, for k_z / k_x values of 0.5 and 0.25, the inflow rates decrease by approximately 1.2 to 1.3 times with each decrement in the anisotropic hydraulic conductivity ratio. The inflow rate for $k_z / k_x = 1$ is 3 times the inflow rate for $k_z / k_x = 0.25$. For a circular tunnel, the inflow rate for $k_z / k_x = 1$ is 2-2.3 times the inflow rate for $k_z / k_x = 0.25$ (Li et al., 2021). This shows that the anisotropic hydraulic conductivity ratio significantly influences the groundwater flow into rectangular tunnels compared to circular tunnels.

4. Illustrative example

A rectangular tunnel with dimensions 5 m in width and 4 m in height is constructed at a depth of 18 m below the groundwater table in a sandy homogeneous soil mass.

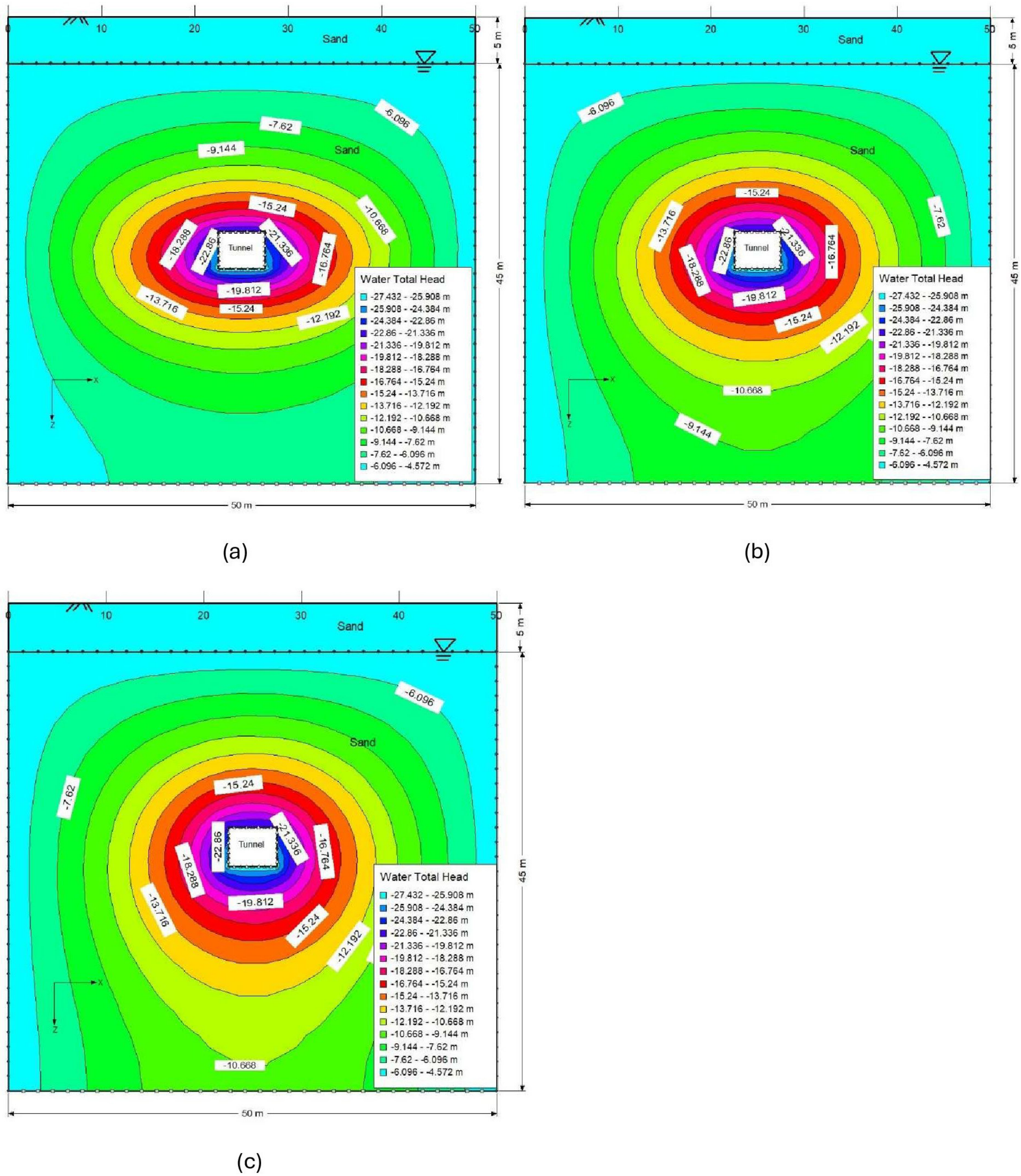

Figure 8. Hydraulic head distribution around tunnel for (a) k_z / k_x =0.25; (b) $k_z / k_x = 0.50$; (c) $k_z / k_x = 0.75$.

The tunnel runs for a length of 60 m. Given that, k_z =1.0 × 10^{-3} m/s. Estimate the total seepage discharge (Q) into the tunnel when $k_z / k_x = 0.75$

Solution:

Given: Width, B = 5 m height, H = 4 m and depth of tunnel below the groundwater table = 18 m

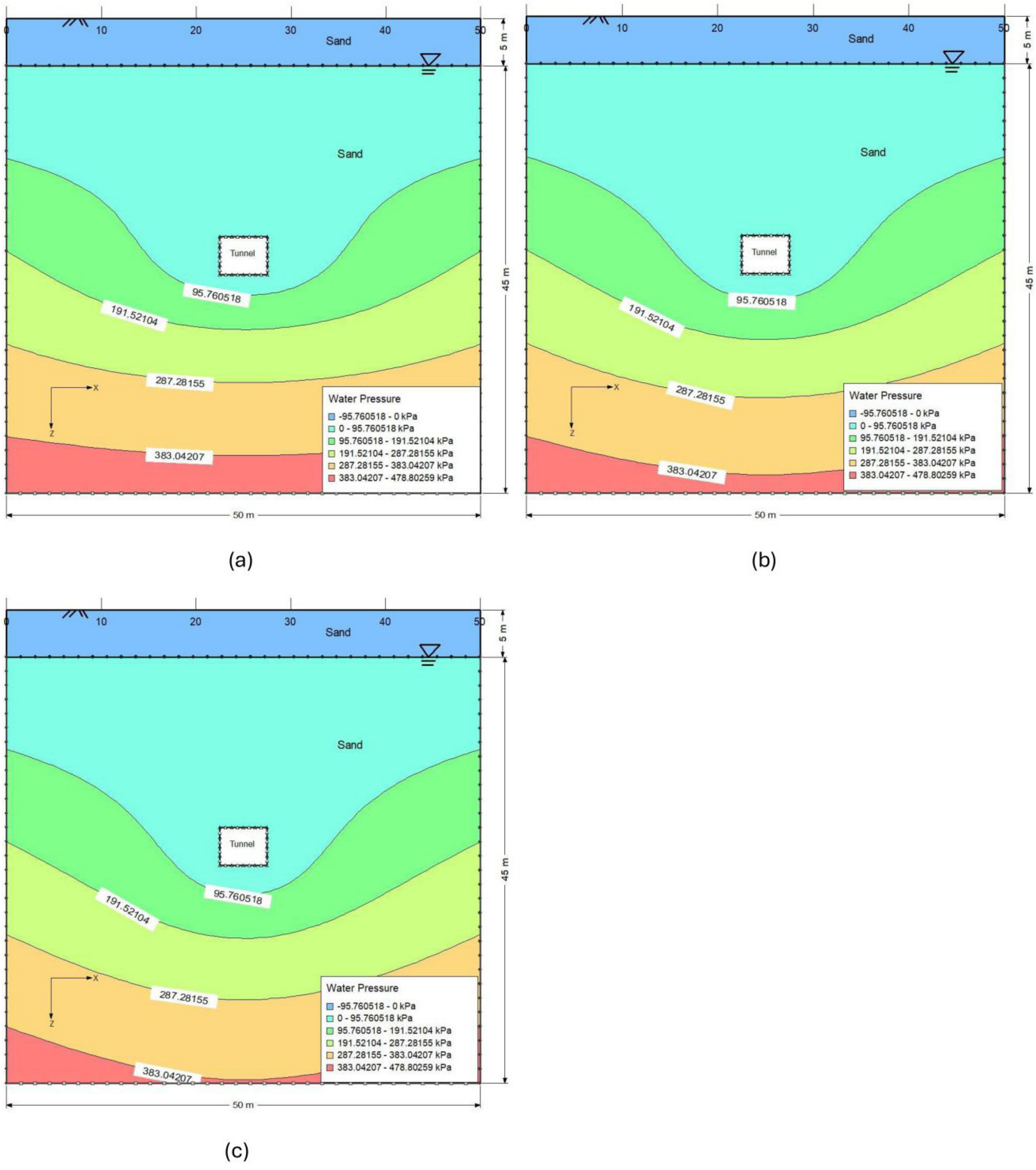

Figure 9. Pore water pressure distribution around tunnel for: (a) $k_z / k_x = 0.25$; (b) $k_z / k_x = 0.50$; (c) $k_z / k_x = 0.75$.

From Figure 12, for $k_z / k_x = 0.75$, the total water inflow rate per meter length of the tunnel, $q = 28 \times 10^{-3}$ m^3/s

Hence, the total seepage discharge into the tunnel, $Q = 60 \times 28 \times 10^{-3} = 1.68$ m^3/s or 1680 l/s

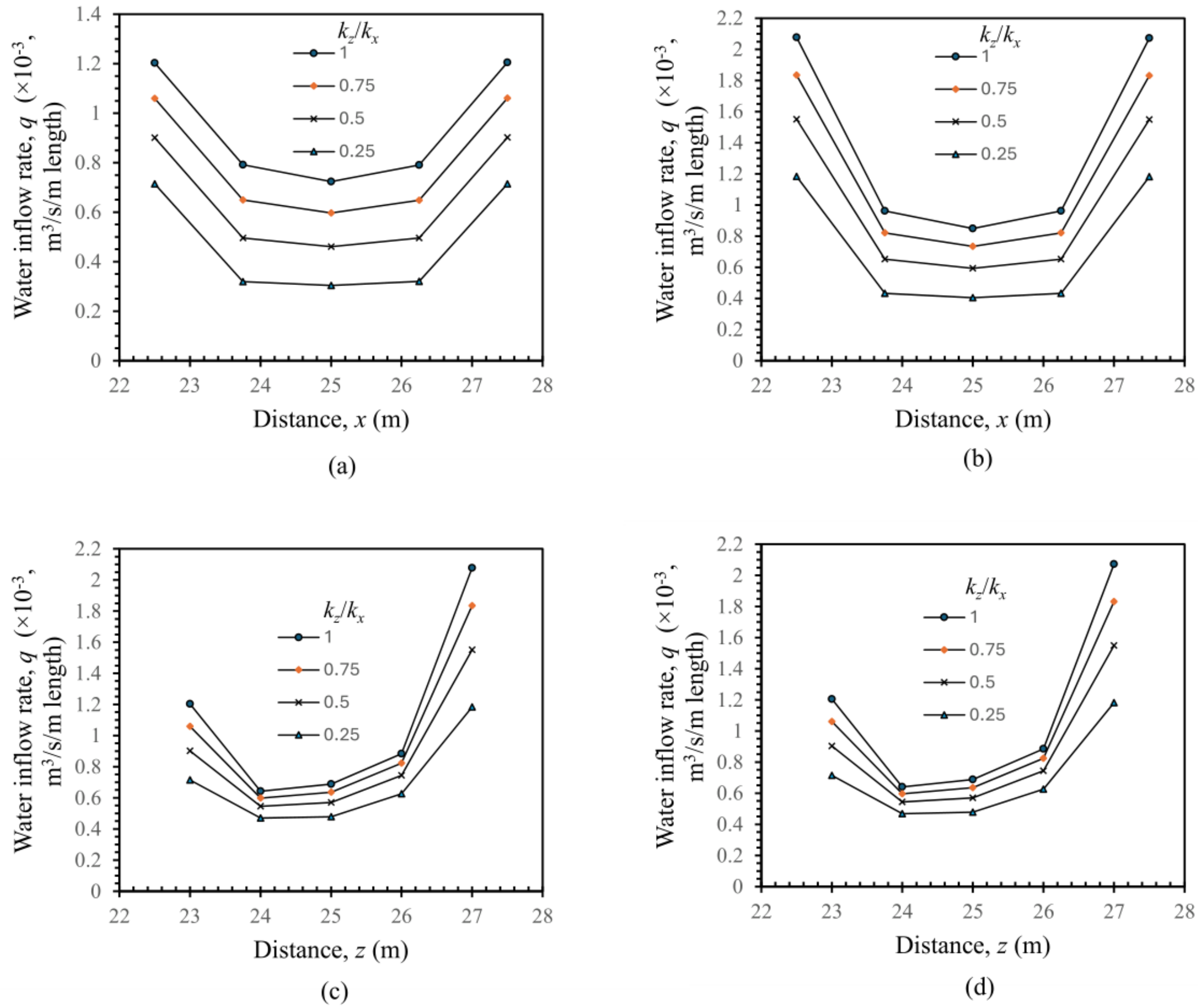

Figure 10. Water inflow rates at the tunnel: (a) crown; (b) invert; (c) left side wall; (d) right side wall

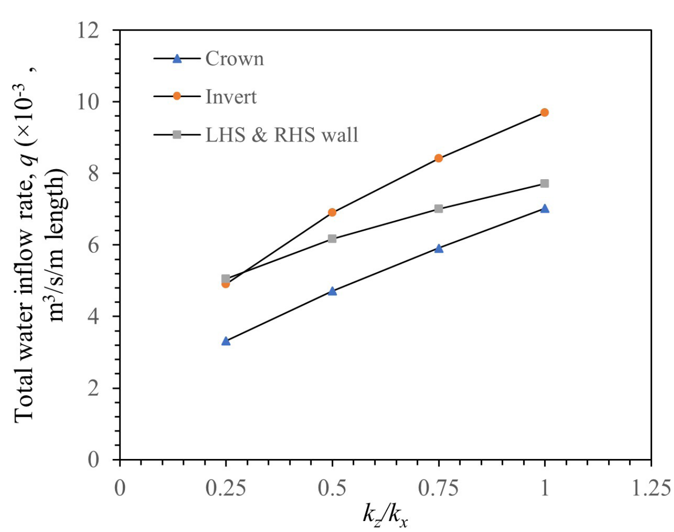

Figure 11. Variation of water inflow rate with anisotropic hydraulic conductivity ratio at different tunnel sections.

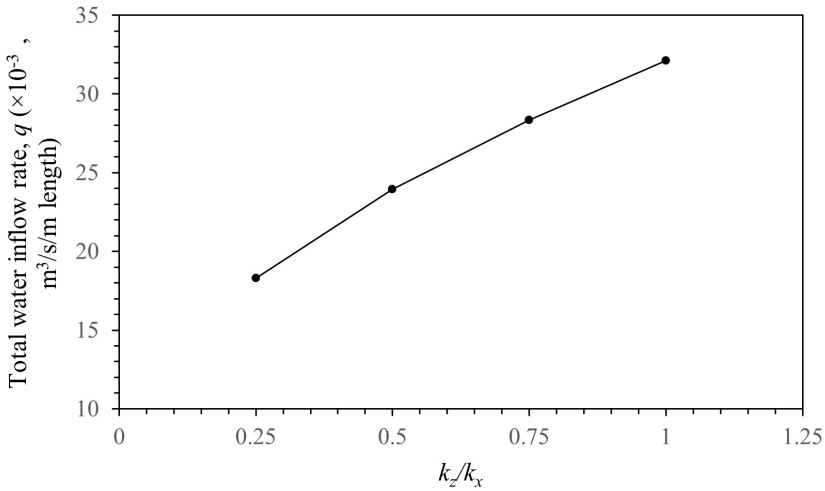

Figure 12. Variation of total water inflow rate with anisotropic hydraulic conductivity ratio.

Similarly, the total seepage discharge can be calculated using the graphical presentation as the design chart for other anisotropic hydraulic conductivity ratios.

5. Conclusions

A numerical analysis was carried out to investigate the effects of the anisotropic hydraulic conductivity ratio on the water inflow rates into a rectangular tunnel located in a saturated homogeneous sand mass. Based on the results and discussion presented earlier, the following conclusions can be drawn:

- As the anisotropic hydraulic conductivity ratio, k_z / k_x, decreases, with horizontal hydraulic conductivity higher than vertical hydraulic conductivity, the hydraulic head and pore water pressure contours become more densely spaced in the horizontal direction. This indicates a steeper hydraulic gradient in that direction, showing the increased effect of horizontal hydraulic conductivity on groundwater flow patterns around the tunnel.
- The invert experiences the highest inflow rate across all k_z / k_x values. This shows that the groundwater pressure below the tunnel contributes significantly to water infiltration from the invert due to gravity and pressure exerted by groundwater below the tunnel.
- The tunnel walls experience a moderate inflow rate, lower than the invert but higher than the crown, which is influenced by horizontal and vertical hydraulic conductivity.
- The crown consistently experiences the lowest inflow rate, meaning it is less impacted by direct groundwater pressure.
- The inflow rate for $k_z / k_x = 1$ is 3 times the inflow rate for $k_z / k_x = 0.25$. This implies that anisotropic hydraulic conductivity significantly impacts inflow rates, with higher horizontal hydraulic conductivity leading to reduced inflow rates around all tunnel sections.
- The relationship between inflow rate and k_z / k_x is approximately linear, indicating a consistent reduction in the inflow rate as the anisotropic ratio decreases. This linear trend highlights the predictability of inflow changes with varying hydraulic conductivity ratios, which can be beneficial in designing effective seepage control methods.
- Recognizing the effect of anisotropic hydraulic conductivity on water inflow is important for tunnel design, particularly in soils with high horizontal hydraulic conductivity. Anticipating more significant inflows at the invert and designing tunnel lining or permanent drainage systems accordingly can mitigate potential seepage issues, leading to its effective management around underground structures.

Hence, anisotropy of the soil mass plays a vital role in groundwater inflow characteristics around tunnels, with higher horizontal hydraulic conductivity significantly reducing the inflow into tunnels. These findings emphasize the need to consider anisotropic soil properties in seepage analysis to optimize tunnel design, as most existing solutions do not consider it, often leading to a conservative design of lining and permanent drainage systems.

Acknowledgements

The authors would like to thank Edith Cowan University, Western Australia, for all the support rendered to carry out this research.

Declaration of interest

The authors have no conflicts of interest to declare. All co-authors have observed and affirmed the contents of the paper and there is no financial interest to report.

Authors' contributions

Deki Yangzom Ghaley: conceptualization, methodology, software, formal analysis, data curation, visualization, writing – original draft. Sanjay Kumar Shukla: conceptualization, supervision, validation, writing – review and editing.

Data availability

All data produced or examined in the course of the current study are included in this article.

Declaration of use of generative artificial intelligence

This work was prepared without the assistance of any generative artificial intelligence (GenAI) tools or services. All aspects of the manuscript were developed solely by the authors, who take full responsibility for the content of this publication.

List of symbols and abbreviations

a	Side length, m
h	Total hydraulic head, m
h_0	Distance of the center of the tunnel from the groundwater table, m
i	Hydraulic gradient
k	Hydraulic conductivity, m/s
k_z	Vertical hydraulic conductivity, m/s
k_x	Horizontal hydraulic conductivity, m/s
q	Specific discharge/water inflow rate, m^3/s
r	Tunnel radius, m

References

Aysen, A. (2006). *Soil mechanics: basic concepts and engineering applications*. London: Taylor & Francis.

Bear, J. (1972). *Dynamics of fluids in porous media.* New York: Dover Publications.

Budhu, M. (2007). *Soil mechanics and foundations.* Chichester: John Wiley & Sons.

Butscher, C. (2012). Steady-state groundwater inflow into a circular tunnel. *Tunnelling and Underground Space Technology*, 32, 158-167. https://doi.org/10.1016/j.tust.2012.06.007.

Butscher, C., Huggenberger, P., Zechner, E., & Einstein, H.H. (2011a). Relation between hydrogeological setting and swelling potential of clay-sulfate rocks in tunneling. *Engineering Geology*, 122(2-4), 204-214. https://doi.org/10.1016/j.enggeo.2011.05.009.

Das, B.M., & Sobhan, K. (2012). *Principles of geotechnical engineering.* Boston: Cengage.

Dong, X., Karrech, A., Basarir, H., Elchalakani, M., & Qi, C. (2020). Closed-form solution to the poromechanics of deep arbitrary-shaped openings subjected to rock mass alteration. *International Journal of Geomechanics*, 20(12), 04020223. https://doi.org/10.1061/(ASCE)GM.1943-5622.0001875.

El Tani, M. (1999). Water inflow into tunnels. In *Proceedings of the World Tunnel Congress ITA-AITES 1999* (pp. 61-70), Oslo. Balkema.

El Tani, M. (2003). Circular tunnel in a semi-infinite aquifer. *Tunnelling and Underground Space Technology*, 18(1), 49-55. https://doi.org/10.1016/S0886-7798(02)00102-5.

Farhadian, H., Aalianvari, A., & Katibeh, H. (2012). Optimization of analytical equations of groundwater seepage into tunnels: a case study of Amirkabir tunnel. *Journal of the Geological Society of India*, 80(1), 96-100. https://doi.org/10.1007/s12594-012-0122-z.

Font-Capo, J., Vázquez-Suñé, E., Carrera, J., Martí, D., Carbonell, R., & Pérez-Estaun, A. (2011). Groundwater inflow prediction in urban tunneling with a tunnel boring machine (TBM). *Engineering Geology*, 121(1-2), 46-54. https://doi.org/10.1016/j.enggeo.2011.04.012.

Freeze, R.A., & Cherry, J.A. (1979). *Groundwater*. Englewood Cliffs: Prentice-Hall.

GEO-SLOPE. (2015). *Seepage modeling with SEEP/W: user's guide*. Calgary: GEO-SLOPE International Ltd.

Goodman, R.E., Moye, D., Schalkwyk, A., & Javendel, I. (1965). Groundwater inflow during tunnel driving. *Engineering Geology*, 1, 150-162.

Harr, M.E. (1962). *Groundwater and seepage.* New York: McGraw-Hill.

Ishibashi, I., & Hazarika, H. (2010). *Soil mechanics fundamentals*. Boca Raton: CRC Press.. https://doi.org/10.1201/b16655.

Karlsrud, K. (2001). *Water control when tunnelling under urban areas in the Olso region* (NFF Publication, No. 12, pp. 27-33). Oslo: NFF.

Kolymbas, D., & Wagner, P. (2007). Groundwater ingress to tunnels-the exact analytical solution. *Tunnelling and Underground Space Technology*, 22(1), 23-27. https://doi.org/10.1016/j.tust.2006.02.001.

Lee, I., & Nam, S. (2001). The study of seepage forces acting on the tunnel lining and tunnel face in shallow tunnels. *Tunnelling and Underground Space Technology*, 16(1), 31-40. https://doi.org/10.1016/S0886-7798(01)00028-1.

Lee, I., Nam, S., & Ahn, J. (2003). Effect of seepage forces on tunnel face stability. *Canadian Geotechnical Journal*, 40(2), 342-350. https://doi.org/10.1139/t02-120.

Lei, S. (1999). An analytical solution for steady flow into a tunnel. *Ground Water*, 37(5), 643. PMid:19125915. https://doi.org/10.1111/j.1745-6584.1999.tb01154.x.

Li, L., Chen, H., Li, J., & Sun, D. (2021). A semi-analytical solution to steady state groundwater inflow into a circular tunnel considering anisotropic permeability. *Tunnelling and Underground Space Technology*, 116, 104115. https://doi.org/10.1016/j.tust.2021.104115.

Liu, J., & Li, X. (2021). Analytical solution for estimating groundwater inflow into lined tunnels considering waterproofing and drainage systems. *Bulletin of Engineering Geology and the Environment*, 80(9), 6827-6839. https://doi.org/10.1007/s10064-021-02378-0.

Ma, J., He, S., Cui, G., He, J., & Liu, X. (2023). Construction stability and reinforcement technology for the super-large rectangular pipe-jacking tunnel passing beneath the operational high-speed railway in composite stratum. *Geomatics, Natural Hazards & Risk*, 14(1), 2208720. https://doi.org/10.1080/19475705.2023.2208720.

Ma, P., Zhao, Y., Shimada, H., & Zhou, H. (2024). Effectiveness analysis of a novel rectangular tunnel boring machine with planetary transmission for box jacking. *Scientific Reports*, 14(1), 27059. PMid:39511272. https://doi.org/10.1038/s41598-024-78206-8.

Muskat, M. (1937). *The flow of homogeneous fluids through porous media.* New York: McGraw-Hill.

Nova, R. (2010). *Soil mechanics.* Hoboken: Wiley.

Park, K., Owatsiriwong, A., & Lee, J. (2008). Analytical solution for steady state groundwater inflow into a drained circular tunnel in a semi-infinite aquifer: a revisit. *Tunnelling and Underground Space Technology*, 23(2), 206-209. https://doi.org/10.1016/j.tust.2007.02.004.

Powrie, W. (2017). *Soil mechanics: concepts and applications*. Boca Raton: CRC Press.

Rat, M. (1973). Ecoulement et répartition des pressions interstitielles autour des tunnels. *Bulletin de Liaison des Laboratoires des Ponts et Chaussées*, (68), 109-124.

Rocscience Inc. (2023). *Application of the finite element method to slope stability.* Toronto.

Schleiss, A.J. (1988). Design of reinforced concrete-lined pressure tunnels. In *Proceedings of the International Congress of Tunnels and Water* (Vol. 2, pp. 1127-1133), Madrid. Balkema.

Shukla, S.K. (2014). *Core principles of soil mechanics.* London: ICE Publishing.

Shukla, S.K. (2025). *ICE core concepts: soil mechanics* (2nd ed.). Bingley: Emerald Publishing.

Smith, M.J. (1981). *Soil mechanics*. New York: Routledge.

Smith, M.J. (2013). *Soil mechanics.* London: Routledge.

Su, K., Zhou, Y., Wu, H., Shi, C., & Zhou, L. (2017). An analytical method for groundwater inflow into a drained circular tunnel. *Ground Water*, 55(5), 712-721. https://doi.org/10.1111/gwat.12513.

Terzaghi, K., Peck, R.B., & Mesri, G. (1996). *Soil mechanics in Engineering practice*. New York: John Wiley & Sons.

Wei, F., Wang, H., Zeng, G., & Jiang, M. (2022). Seepage flow around twin circular tunnels in anisotropic ground revealed by an analytical solution. *Underground Space*, 10, 1-14. https://doi.org/10.1016/j.undsp.2022.08.003.

Yang, G., Wang, X., Wang, X., & Cao, Y. (2015). Analyses of seepage problems in a subsea tunnel considering effects of grouting and lining structure. *Marine Georesources and Geotechnology*, 34(1), 65-70. https://doi.org/10.1080/1064119X.2014.958882.